Lone-pair effects and structural trends in $x\,SnO\cdot(1-x)\,P_2O_5$ glasses deduced from ^{31}P and ^{119}Sn nuclear magnetic resonance

2002 J. Phys.: Condens. Matter 14 13609

(http://iopscience.iop.org/0953-8984/14/49/315)

INSTITUTE OF PHYSICS PUBLISHING JOURNAL OF PHYSICS: CONDENSED MATTER

J. Phys.: Condens. Matter **14** (2002) 13609–13621 PII: S0953-8984(02)52100-7

Lone-pair effects and structural trends in $x\mathrm{SnO}\cdot(1-x)\mathrm{P_2O_5}$ glasses deduced from ^{31}P and ^{119}Sn nuclear magnetic resonance

D Holland[1], A P Howes[1], M E Smith[1] and A C Hannon[2]

[1] Department of Physics, University of Warwick, Coventry CV4 7AL, UK
[2] ISIS, Rutherford Appleton Laboratory, Chilton, Didcot, UK

Received 7 August 2002
Published 29 November 2002
Online at stacks.iop.org/JPhysCM/14/13609

Abstract

Tin phosphate glasses, of general formula $x\mathrm{SnO}\cdot(1-x)\mathrm{P_2O_5}$ ($0.3 < x < 0.8$), have been prepared by conventional melt-quench techniques and their structures studied using ^{31}P and ^{119}Sn nuclear magnetic resonance. The distribution of $[\mathrm{PO_4}]$ Q^n species changes with composition in accordance with the simple binary model, and the changes in chemical shift can be explained by the redistribution of electron charge from the P=O double bond. Sn(II) is found to occupy a highly asymmetric site, typical of a sterically active lone pair of electrons. The ^{119}Sn parameters of the chemical shift tensor change systematically with x, reflecting the change in local environment from one where the next nearest neighbours are predominantly Q^2 phosphorus to one where they are predominantly Q^0 phosphorus.

1. Introduction

Interest in glasses containing tin oxide has been fuelled by the drive to find substitutes for the environmentally unwelcome lead analogues. There is also an increasing awareness that glasses in which a significant component is a 'lone-pair' cation can possess useful nonlinear optical properties. It is well known that the nonbonding ('lone') pair of electrons on Sn(II) ions is sterically active and results in highly asymmetric Sn(II) environments in crystalline oxide compounds such as SnO [1] and $\mathrm{Sn_3P_2O_8}$ [2]. Recent work has shown that this lone pair appears to remain sterically active even when incorporated in an amorphous network [3–5] and the Sn–O coordination number is reduced from four to three. Direct evidence for this comes from ^{119}Sn nuclear magnetic resonance (NMR) and Mössbauer spectroscopies where lineshapes characteristic of highly asymmetric environments are obtained, and from neutron diffraction which provides information on coordination numbers. A better understanding of this asymmetry is needed if we are to understand how physical properties are affected by composition and also network type. To this end, we are engaged in measuring the chemical shift tensor parameters in glasses and related crystalline compounds.

Table 1. Glass compositions expressed as nominal mole fraction (x_{nom}) of SnO in $x\mathrm{SnO}(1-x)\mathrm{P_2O_5}$; as determined by difference using quantitative ^{31}P NMR (x_{an}); and expressed as x' from $x'\mathrm{SnO}\ (1-x')\mathrm{PO_{2.5}}$ using analysed values. The atomic fraction of H present was determined by quantitative ^{1}H NMR and has been neglected in subsequent calculations involving composition. The densities were determined by Archimedes' method (ρ_b) and by pycnometry (ρ_{pyc}) and have been converted into the respective molar volumes (MV) using x_{an}.

Sample	x_{nom}	$x_{an} \pm 0.02$	ρ_b (g cm^{-3})	ρ_{pyc} (g cm^{-3})	x'	MV$_b \pm 0.01$ (cm^3 mol^{-1})	MV$_{pyc} \pm 0.01$ (cm^3 mol^{-1})	H (at. frac.)
P_2O_5 [17]	0		2.445		0		29.03	
P_2O_5 [18]	0		2.385		0		29.76	
sn30	0.30	0.37	3.024	3.136	0.23	28.32	27.30	0.008
sn30f	0.30	0.32	3.036	3.112	0.19	27.37	26.69	
sn40	0.40	0.44	3.177	3.224	0.28	27.97	27.55	0.007
sn50	0.50	0.5	3.337	3.369	0.33	27.58	27.31	0.01
sn50f	0.50	0.49	3.236	3.352	0.32	28.23	27.25	
sn60	0.60	0.6	3.517	3.56	0.43	27.97	27.63	0.0
sn67	0.667	0.69	3.722	3.766	0.53	28.14	27.81	
sn70	0.70	0.68	3.937	3.96	0.52	26.44	26.29	0.008
sn70f	0.70	0.68	3.912	3.955	0.5	26.61	26.32	0.0
sn75	0.75	0.73	4.152		0.57	25.84		
sn80	0.80	0.79			0.65			
SnO	1		5.59		1.00			

Reviews of the structures of v-P_2O_5 [6] and phosphate glasses [7] describe how the P=O double bond, which is present in v-P_2O_5, lengthens with addition of modifier oxides and gradually becomes indistinguishable from other P–O bonds, i.e. the charge on a nonbridging oxygen is delocalized over the entire [PO_4] tetrahedron. This has been represented conceptually by the use of the bond order descriptor [8]. The use of NMR to study phosphate glasses has been recently reviewed by Brow [9] and Hoppe [7] has similarly reviewed diffraction studies of phosphate glasses. This paper reports the effects of incorporating SnO on the ^{31}P NMR parameters in tin phosphate glasses.

2. Experiment

2.1. Sample preparation

Samples were prepared from SnO and $NH_4H_2PO_4$. A small quantity (0.1 mol%) of Fe_2O_3 was also added to the batch to reduce the relaxation time of the ^{119}Sn nuclei in the NMR experiments. The stoichiometric quantities to produce compositions $x\mathrm{SnO}(1-x)\mathrm{P_2O_5}$ for $x = 0.3$–0.8 (table 1) were ground together and heated in silica crucibles to 1000–1100 °C, depending on composition, holding for 1 h at 600 °C during the heating cycle to allow removal of NH_3 and H_2O. The samples were held at the maximum temperature for 1 h to ensure all these volatiles were gone and the melt was then quenched between copper plates to produce glass samples ∼1 mm thick. After quenching, the samples were transferred immediately to a desiccator to avoid reaction with atmospheric moisture—a significant problem for glasses with P_2O_5 content greater than 50 mol%.

Since samples with high P_2O_5 content (low x) were subject to loss of P_2O_5 by volatilization at the melting temperature, as well as moisture attack, the compositions of the glasses were determined by quantitative ^{31}P and ^{1}H NMR, giving the P_2O_5 and H_2O contents.

The SnO content was then obtained by difference. There was no evidence of attack on the silica crucible and no silicon could be detected in the resulting glasses using energy dispersive x-ray analysis.

Since Sn(II) is thermodynamically unstable with respect to Sn(IV), some conversion can occur during melting by either oxidation or disproportionation. There was no evidence of disproportionation under the conditions used but some oxidation resulted in the formation of a crystalline 'crust' at the meniscus between the melt and the crucible. Care was needed when pouring the glass to avoid entrainment of this crystalline material in the glass. Any such contamination was removed mechanically before subsequent experiments. Samples labelled *f* in table 1 are repeat preparations of some compositions with the addition of 1 wt% carbon to attempt to control oxidation. X-ray diffraction was used to check the amorphous nature of the materials.

2.2. Physical property determination

Sample densities were obtained for both bulk and powder samples so that any porosity could be identified and quantified—this can be a problem with viscous melts from which volatiles are being evolved. The bulk measurements were performed using Archimedes' method with 1,1,1-trichloroethane as the displacement fluid. The powder measurements were performed by helium displacement using a micropycnometer.

2.3. Nuclear magnetic resonance

Magic-angle-spinning (MAS) spectra were obtained, on a CMX360 spectrometer, using a Doty probe with a 4 mm rotor for ^{31}P and a Chemagnetics probe with a 6 mm rotor for ^{1}H. Proton spectra were acquired at 360 MHz, using a pulse length of 4 μs ($\pi/2$), a pre-acquisition delay of 40 μs and a delay of 1 s. The sample was spun at 3 kHz and adamantane ($C_{10}H_{16}$) was used to calibrate the system to allow quantification. The proton spectra were collected for known masses of samples, and the tuning of the system was reproduced as closely as possible each time. The proton background was then measured, for the same number of acquisitions, on an empty rotor and subtracted from the sample spectra before comparison with the signal from a known mass of $C_{10}H_{16}$, scaled to the same number of acquisitions. The phosphorus spectra were obtained at 145.78 MHz, with a pulse length of 2 μs ($\pi/4$), a pre-acquisition delay of 15 μs and a delay of 30 s. The combination of short pulse length and the presence of paramagnetic Fe^{3+} means that a delay of 30 s was found to be sufficient to ensure full relaxation and hence quantitative spectra. The samples were spun at 10 kHz and were referenced to $NH_4H_2PO_4$ (chemical shift 0.8 ppm w.r.t. 85% H_3PO_4). To quantify the amount of P_2O_5 in each glass, the NMR samples were weighed and the integrated ^{31}P signal compared with that from a known quantity of $NH_4H_2PO_4$ (acquired with a pulse delay of 600 s). The ^{119}Sn NMR spectra were acquired static on a CMX240 spectrometer at 88.74 MHz. The pulse length was 2 μs and the pulse delay 25 s. Aqueous $SnCl_2$ was used as the reference with solutions being prepared fresh for each run.

3. Results and discussion

3.1. Samples

Most samples were amorphous to x-rays but small Bragg peaks were visible in the $x = 0.44$ and 0.50 samples (figure 1). The crystalline phase was identified as SnP_2O_7 (with possible traces of SnO_2 and $Sn_2P_2O_7$), i.e. it results from oxidation of Sn(II) to Sn(IV) which is precipitated

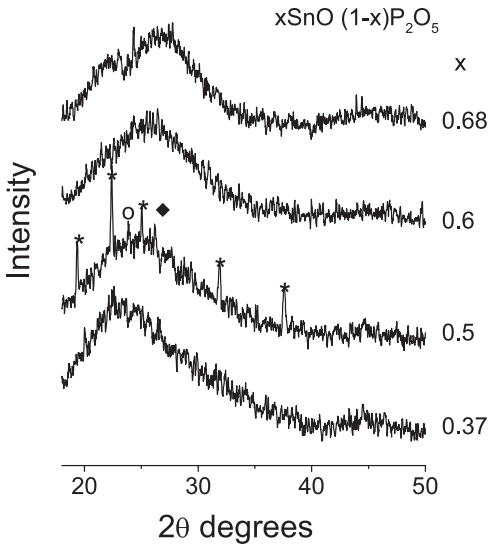

Figure 1. X-ray diffraction patterns from the xSnO $(1-x)P_2O_5$ glasses prepared by melt quenching. Some devitrification can be seen in the $x = 0.5$ sample, giving largely SnP_2O_7(∗) with traces of $Sn_2P_2O_7$ (○) and SnO_2 (♦).

from the glass as tin(IV) pyrophosphate. It is not obvious whether SnO_2 first forms and then reacts with P_2O_5 or whether the tin(II) pyrophosphate forms and then oxidizes—the former seems more likely. The physical appearance of the samples was generally that of clear glasses but there was some trace of opalescence in the $x = 0.44$ and 0.50 samples which may be a consequence of the presence of crystal phase but may also suggest that glass-in-glass phase separation occurs at these concentrations and possibly precedes devitrification. Bubbles were also visible in some samples.

The densities obtained by bulk measurement were somewhat lower than those obtained from pycnometry of the powdered samples and the differences observed were consistent with porosities up to 1.4% by volume (table 1). Figure 2 shows how the density varies with SnO content. It is expected that tin–oxygen polyhedra effectively replace phosphorus–oxygen polyhedra. Consequently, it is more logical to look at variations of properties by expressing the composition in terms of $PO_{2.5}$ such that the SnO content is now expressed as x' in x'SnO$(1 - x')PO_{2.5}$ where $x' = x/(2 - x)$. This also enables direct comparison with other network systems such as SiO_2 and GeO_2. Certainly the dependence of density upon x' is more closely linear than its variation with x.

The sample compositions deduced from quantitative ^{31}P NMR are summarized in table 1 and expressed as both x and x'. Samples prepared with the inclusion of 1 wt% C showed no difference in any property for $x = 0.50$ and 0.68 but there were significant differences for $x = 0.32$—largely the result of reduced loss of P_2O_5 by volatilization.

3.2. Nuclear magnetic resonance

3.2.1. ^{1}*H NMR.* The proton contents of those glasses analysed by NMR are given in table 1. These concentrations are not considered of sufficient significance to require their inclusion in any subsequent discussions of structure.

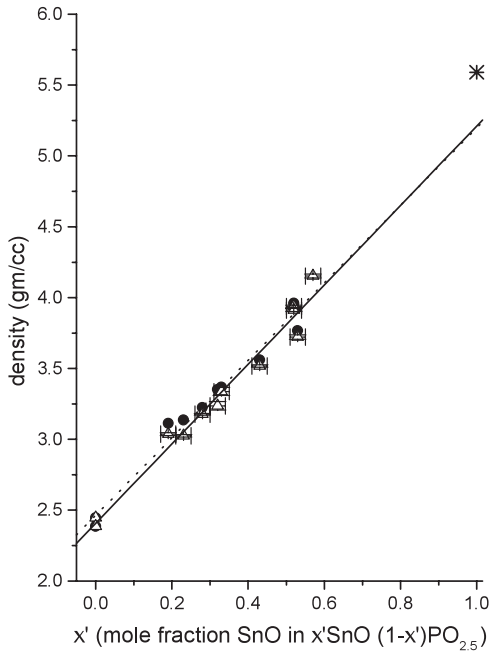

Figure 2. Variation of glass density as a function of x' in x'SnO $(1-x')$PO$_{2.5}$. Error bars are shown for the bulk density measurements (Δ) and are smaller than the symbol used for the pycnometer measurements on powder ($\bullet$). $*$ indicates the density of c-SnO. The dotted and solid lines are the straight line fits to the pycnometer and bulk data respectively.

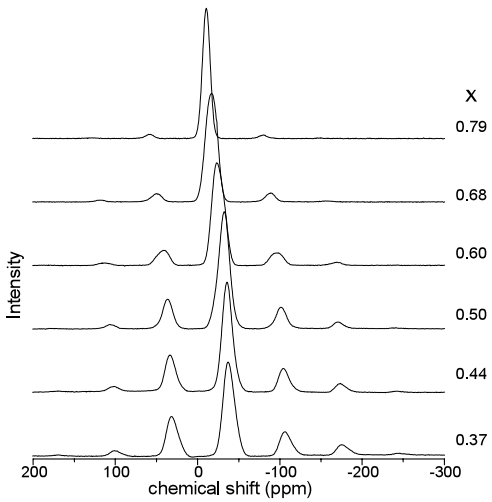

Figure 3. ^{31}P MAS NMR spectra obtained from the glasses. The chemical shift is with respect to H_3PO_4.

3.2.2. ^{31}P NMR. ^{31}P MAS NMR spectra are shown in figure 3 where the sideband intensity distribution illustrates the increase in the [PO_4] site symmetry as the amount of SnO is increased and, ultimately, all [PO_4] units become isolated orthophosphate. In figure 4, the spectra are expanded to show only the isotropic peak. The position of the peak maximum moves

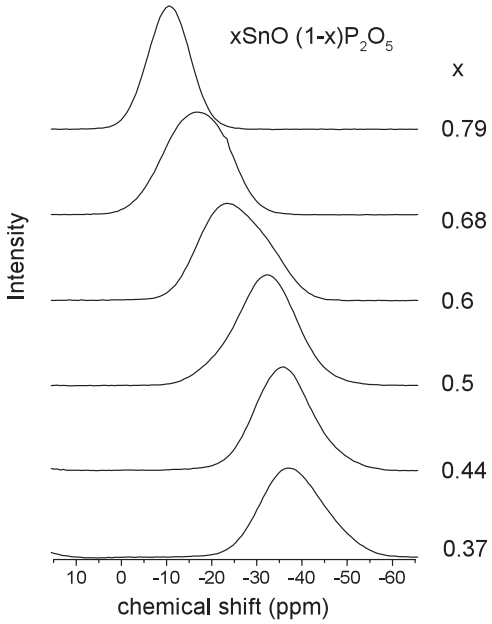

Figure 4. ^{31}P MAS NMR spectra expanded to show only the main peak shape. The chemical shift is with respect to H_3PO_4.

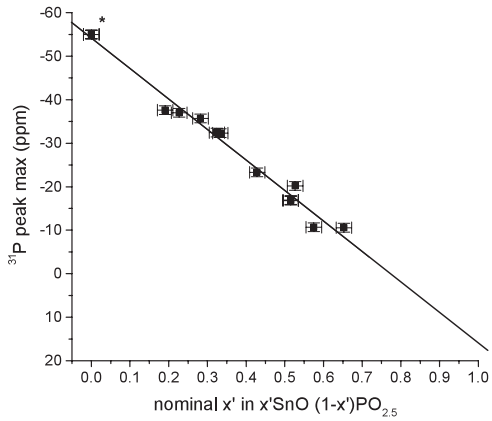

Figure 5. Change in ^{31}P peak maximum with x' in $x'\mathrm{SnO}(1-x')\mathrm{PO}_{2.5}$. The chemical shift is with respect to H_3PO_4. (* Value for v-P_2O_5 from [19].)

systematically with increasing SnO content from −38 to −10 ppm (figure 5), indicating reduced shielding of the phosphorus nucleus as the phosphate network becomes increasingly depolymerized. The asymmetry of the isotropic peak in many of the samples indicates the presence of more than one site and therefore all spectra were fitted with contributions from two species using Gaussian lineshapes and included the spinning sidebands in the fitting procedure. Example fits are shown in figure 6 and the results of the fits, in terms of peak positions, peak widths and site populations, are summarized in table 2.

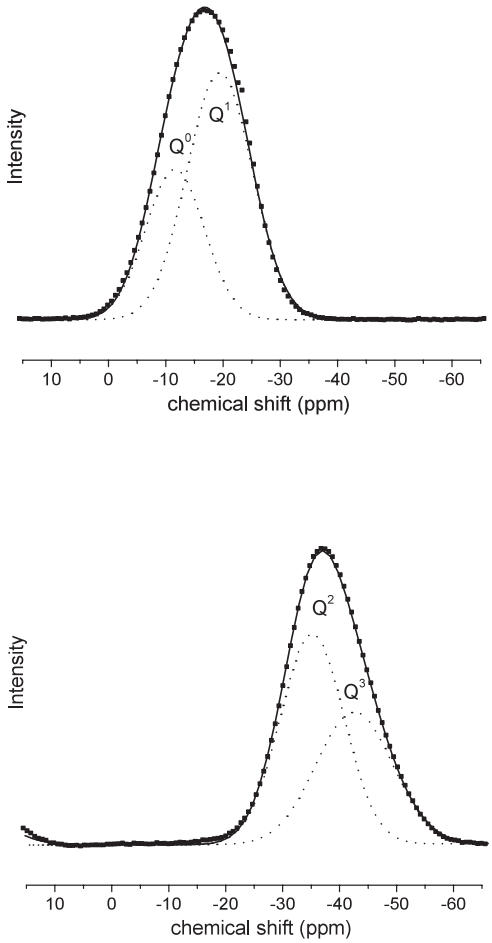

Figure 6. Gaussian fits to the main ^{31}P peaks of the $x = 0.37$ (lower) and $x = 0.79$ (upper) samples. Points are data, the solid curve is the total fit and the dotted curves are the individual Q species contributions to the fit. The chemical shift is with respect to H_3PO_4.

The Q distribution can be modelled as a simple binary distribution assuming that each SnO replaces two P–O–P links by two P–O–Sn which we can write as

$$2Q^n + \mathrm{SnO} \rightarrow 2Q^{n-1}. \tag{1}$$

Thus, different Q species are formed by this successive replacement, with no more than two species being present at any composition.

The ultraphosphate region ($0 \leqslant x \leqslant 0.50$) gives a mixture of Q^2 and Q^3 species whose fractions are given by

$$f(Q^2) = \frac{x}{(1-x)} \tag{2a}$$

$$f(Q^3) = \frac{1-2x}{(1-x)}. \tag{2b}$$

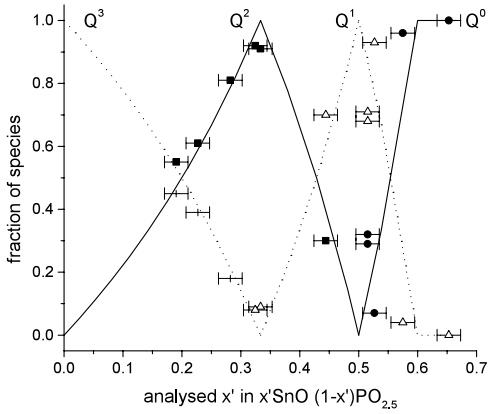

Figure 7. Change in fraction of each Q^n species with x' in x'SnO $(1-x')$PO$_{2.5}$.

Table 2. Spectral parameters obtained from the fitting of ^{31}P NMR spectra: chemical shifts ($\delta \pm 0.1$ ppm) and fractions of Q species ($f(Q^n) \pm 0.02$).

Sample	x_{an}	x'	$\delta(Q^3)$ (ppm)	$\delta(Q^2)$ (ppm)	$\delta(Q^1)$ (ppm)	$\delta(Q^0)$ (ppm)	$f(Q^3)$	$f(Q^2)$	$f(Q^1)$	$f(Q^0)$
v-P_2O_5 [19]	0	0	−55							
sn30	0.37	0.227	−42.6	−35.2			0.39	0.61		
sn30f	0.32	0.190	−42.7	−35.4			0.45	0.55		
sn40	0.44	0.282	−42.7	−34.7			0.18	0.81		
sn50	0.5	0.333		−32.5	−20.3			0.91	0.09	
sn50f	0.49	0.325		−32.6	−20.3			0.92	0.08	
sn60	0.6	0.429		−32.6	−22.7			0.3	0.7	
sn67	0.69	0.527			−20.6	−9.6			0.93	0.07
sn70	0.68	0.515			−19.4	−11.6			0.68	0.32
sn70f	0.68	0.515			−19.4	−11			0.71	0.29
sn75	0.73	0.575			−15.3	−10.5			0.04	0.96
sn80	0.79	0.653				−10.6			0.0	1

The metaphosphate to pyrophosphate ($0.50 \leqslant x \leqslant 0.67$) region gives a mixture of Q^2 and Q^1 species:

$$f(Q^2) = \frac{(2-3x)}{(1-x)} \tag{3a}$$

$$f(Q^1) = \frac{(2x-1)}{(1-x)}. \tag{3b}$$

The pyrophosphate to orthophosphate ($0.67 \leqslant x \leqslant 0.75$) region gives a mixture of Q^1 and Q^0 species:

$$f(Q^1) = \frac{(3-4x)}{(1-x)} \tag{4a}$$

$$f(Q^0) = \frac{(3x-2)}{(1-x)} \tag{4b}$$

and, beyond $x = 0.75$ ($x' = 0.6$), only orthophosphate species are expected. The binary distribution and the observed concentrations of species are compared in figure 7, which demonstrates that the binary model is a reasonable description of this system.

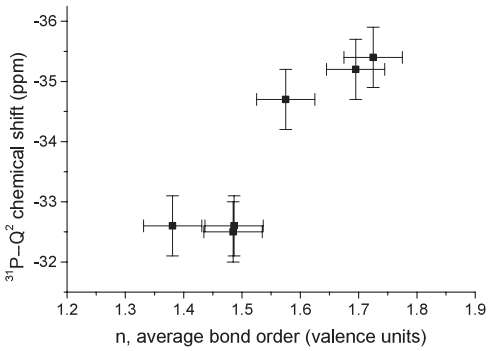

Figure 8. Relationship between Q^2–^{31}P chemical shift and bond order n. The chemical shift is with respect to H_3PO_4.

Van Wazer [10] and Brow *et al* [8, 11] attributed trends in ^{31}P isotropic chemical shift to changes in the average π-character of the P–O bonds as the number of NBOs decreases. Applying the bond strength arguments developed by Brow [8], the valences of the tin (+2) and phosphorus (+5) cations are distributed between the cation–oxygen bonds of a given tetrahedron such that the total of the values assigned to the bonds connected to an oxygen atom must equal two to satisfy the valence requirements of the oxygen atom. Thus, metaphosphate (Q^2) species have two nonbridging P–O$^-$ bonds, each with a bond strength of 1.5 valence units (vu—defined as the charge divided by coordination number); pyrophosphate (Q^1) species have three nonbridging P–O bonds, each assigned 1.33 vu; in orthophosphate (Q^0) species the value is 1.25 and in the branching units (Q^3) the nonbridging P=O bond is assigned 2.0 vu.

The average P–NBO bond order, n (in valence units) can be calculated using equation (5) modified from Brow *et al* [8], where $f(Q)$ are the fractions of given species and an increase in n implies an increase in π bonding.

$$n = 2.0f(Q^3) + 1.5f(Q^2) + 1.33f(Q^1) + 1.25f(Q^0). \tag{5}$$

The ^{31}P–Q^2 chemical shift versus the average P–NBO bond order, n, is shown in figure 8. The deviations from a straight line are more marked than observed in previous studies [12, 13] which may be due to the greater deviations from stoichiometry or the presence of significant amounts of crystal phase in the ∼50 mol% SnO (vu = 1.5) samples. There is a systematic shift to less shielded values as the average bond order, n, decreases, associated with an increasing overall (Sn–O–P)/(P–O–P) ratio and decreasing average charge on P in Q^2-sites. However, it should be noted that the slope of this line is -9.8 ± 2 ppm/valence unit compared to the values of ∼−22 for cadmium phosphates [13] and ∼−50 ppm/valence unit for sodium phosphates [8]. This reflects the fact that the Sn–O bonding has a significant covalent character. Kirkpatrick and Brow [8] compared the ^{31}P shifts for various series of metaphosphate glasses with the cation potential (z/r) for the modifying cation and showed a near linear relationship with shifts becoming more negative (increased shielding) as cation potential increased. They account for this as the result of decreased P–O bond strength as the M–O bond strength increases. Stannous metaphosphate glass is consistent with this trend although the shift is more negative than predicted from the correlation since the z/r values are based on octahedral coordination which is inappropriate for Sn(II). The observed shift value would correspond to a z/r of ∼2.45, close to the values for Zn^{2+} and Mg^{2+}. The authors also commented on the increase in the width of the ^{31}P peak with cation potential which is consistent with the widths observed in this study.

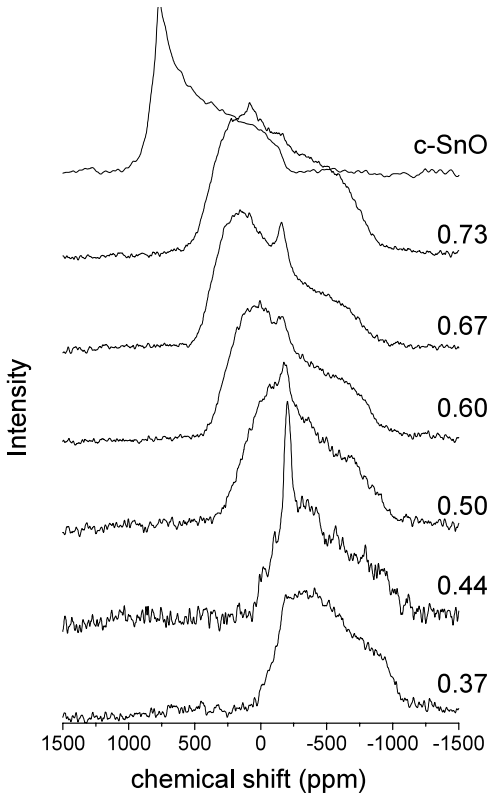

Figure 9. ^{119}Sn static NMR spectra for glasses and c-SnO. The sharper peak at ~ -170 ppm is from Sn(IV) in SnP_2O_7 and the small sharp peak at ~ 0 ppm in the 0.73 sample is from Sn(IV) in SnO_2. The chemical shift is with respect to $SnCl_2$.

3.2.3. ^{119}*Sn NMR.* The ^{119}Sn static NMR spectra from the glass samples are shown in figure 9 and are compared with the spectrum of crystalline SnO. Crystalline SnO_2 gives a relatively narrow ^{119}Sn line associated with the near octahedral disposition of O atoms about Sn(IV), whereas the lineshapes of crystalline SnO and the glass spectra reflect the large chemical shift anisotropy (CSA) associated with the asymmetry of the Sn(II) site. The amount of chemical shift dispersion associated with the Sn(II) line means that it would be impractical to narrow it by MAS. However, significant information can be obtained from the static lineshape, even though closely related sites cannot be resolved. The lineshapes in the ^{119}Sn spectra were fitted [14] to yield values for the principal components of the shift tensor, δ_{11}, δ_{22} and δ_{33}, and hence enable calculation of the isotropic chemical shift ($\delta_{iso} = (\delta_{11} + \delta_{22} + \delta_{33})/3$), span ($\Omega = \delta_{11} - \delta_{33}$) and skew ($\kappa = 3[\delta_{22} - \delta_{iso}]/\Omega$) [15]. The values obtained are summarized in table 3 and plotted as a function of x' in figures 10 and 11.

It is noticeable that the ^{119}Sn isotropic chemical shift in the glasses becomes more positive as x' increases—i.e. it becomes less shielded as it tends towards the value for c-SnO. The possible causes of this are change in next nearest neighbour, change in coordination number, change in hybridization and extent of the lone pair in space. The replacement of next nearest neighbour Sn in SnO by P in the glasses could have an effect on chemical shift, though the greater electronegativity of P might be expected to reduce electron density in the region of the Sn nucleus and therefore reduce shielding, rather than increase it as is observed.

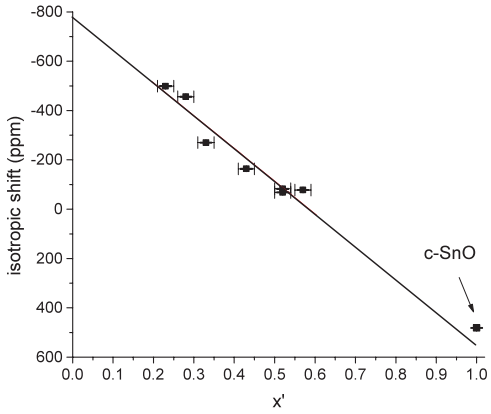

Figure 10. Change in ^{119}Sn isotropic shift with x' in x'SnO $(1-x')$$PO_{2.5}$. The chemical shift is with respect to $SnCl_2$.

Table 3. Spectral parameters from fitting of the ^{119}Sn NMR spectra.

$x \pm 0.02$	$x' \pm 0.02$	δ_{iso} (ppm) ± 5	δ_{11} (ppm) ± 10	δ_{22} (ppm) ± 10	δ_{33} (ppm) ± 10	Span (ppm) ± 20	Skew ± 0.02
0.37	0.23	−499	−77	−406	−1014	937	0.30
0.44	0.28	−456	−12	−335	−1021	1009	0.36
0.50	0.33	−270	173	−138	−845	1018	0.39
0.60	0.43	−164	291	27	−810	1101	0.52
0.68	0.52	−68	387	156	−747	1134	0.59
0.69	0.52	−83	358	155	−762	1120	0.64
0.73	0.57	−78	411	186	−831	1242	0.64
1.0	1.0	481	791	791	−138	929	1.0

However, the electronegativity of P is not much greater than that of Sn and also next nearest neighbour atoms have little direct effect on the shielding of a nucleus, with their influence largely through changes to the Sn–O bonding and hybridization of the 5s, 5p and 5d orbitals of tin. The coordination number of tin in the glass is expected to be three, as observed for other systems, and not the four-coordination of Sn by O observed in c-SnO. Coordination to three oxygen atoms has been previously observed by neutron diffraction in SnO–SiO_2 [16] and SnO–GeO_2 glasses [5] and it is likely that this will also be the case in phosphate glasses. In both the silicate and germanate systems the tin nucleus is more shielded in the glass than in c-SnO, in spite of the lower coordination number. It is usual for lower coordinated nuclei to be *less* shielded than those with higher coordination but in the case of Sn(II) the shielding is likely to be dominated by the lone pair of electrons which can approach more closely to the Sn nucleus when the number of nearest neighbour oxygens is smaller.

The values of skew are seen to increase from 0.3 for $x = 0.37$ to 0.64 for $x = 0.73$ and the straight line fit in figure 11(a) passes close to the value of 1.0 which is observed for c-SnO. This trend reflects the increasing number of Sn atoms in the fourth coordination sphere but may also indicate an increase in Sn–O coordination.

An additional, much narrower, line can be seen in most spectra at ~ -170 ppm. This arises from the devitrification product SnP_2O_7, in which tin is present as Sn(IV). The narrowness of the line is thus largely due to the site symmetry of Sn(IV). This phase is generally present at

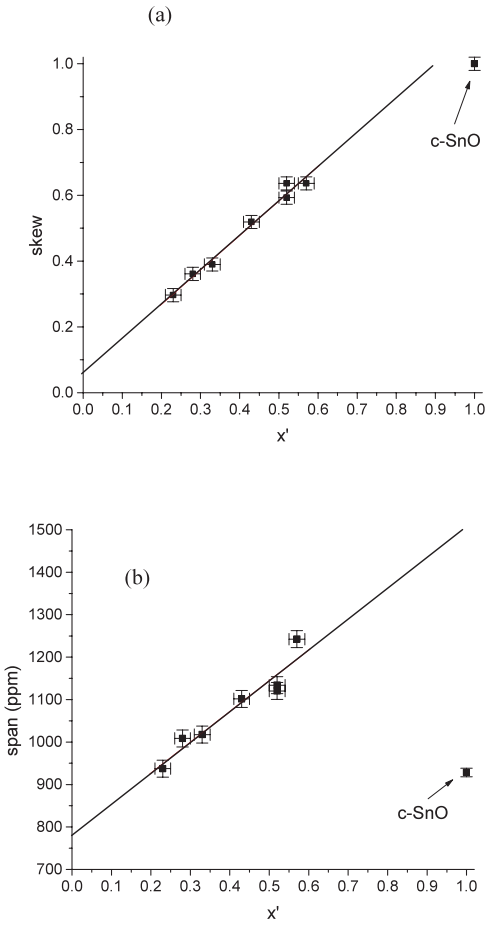

Figure 11. Change in skew and span with x' for ^{119}Sn in glasses of composition x'SnO $(1-x')$PO$_{2.5}$.

2% of total Sn or less and hence not detected by XRD, but in the $x = 0.44$ sample there is 8% of Sn present as crystalline phase.

4. Conclusions

Both ^{119}Sn and ^{31}P chemical shifts become more positive (deshielded) with increase in SnO content and the symmetry of the Sn(II) site increases. This may be accounted for by

(a) the increasing delocalization of charge from the P=O double bond into the other P–O bonds and;
(b) change in the s–p hybridization of the orbitals on Sn such that the lone pair moves closer to the tin nucleus.

If some 5d is included in the hybridization, then an increase in the tin coordination may occur and this would be consistent with the observed increase in the ^{119}Sn skew parameter. Measurements of the Sn–O bond lengths, O–Sn–O bond angles and Sn–O coordination number are required to confirm this.

References

[1] Moore W J and Pauling L 1941 *J. Am. Chem. Soc.* **63** 1392
[2] Mathew M, Schroeder L W and Jordan T H 1982 *Acta Crystallogr.* B **24** 1968
[3] Williams K F E, Johnson C E, Johnson J A, Holland D and Karim M M 1995 *J. Phys.: Condens. Matter* **7** 9485
[4] Johnson J A, Johnson C E, Holland D, Sears A, Bent J F, Appleyard P G, Thomas M F and Hannon A C 2000 *J. Phys.: Condens. Matter* **12** 213
[5] Holland D, Smith M E, Poplett I J F, Johnson J A, Thomas M F and Bland J 2001 *J. Non-Cryst. Solids* **293–295** 175
[6] Martin S W 1991 *Eur. J. Solid State Inorg. Chem.* **28** 163
[7] Hoppe U, Walter G, Kranold R and Stachel D 2000 *J. Non-Cryst. Solids* **263/264** 29
[8] Brow R K, Kirkpatrick R J and Turner G L 1990 *J. Non-Cryst. Solids* **116** 39
[9] Brow R K 2000 *J. Non-Cryst. Solids* **263/264** 1
[10] Van Wazer J R 1967 *Phosphorus and its Compounds* vol 1 and 2 (New York: Interscience)
[11] Brow R K, Tallant D R, Hudgens J J, Martin S W and Irwin A D 1994 *J. Non-Cryst. Solids* **177** 221
[12] Brow R K, Tallant D R, Myers S T and Phifer C C 1995 *J. Non-Cryst. Solids* **191** 45
[13] Hussin R, Holland D and Dupree R 2002 *J. Non-Cryst. Solids* **298** 32
[14] Massiot D, Fayon F, Capron M, King I, Le Calvi S, Alonso B, Durand J-O, Bujoli B, Gan Z and Hoatson G 2002 *Magn. Reson. Chem.* **40** 70
[15] MacKenzie K J D and Smith M E 2002 *Multinuclear Solid State NMR of Inorganic Materials* (Oxford: Pergamon)
[16] Bent J F, Hannon A C, Holland D and Karim M M A 1998 *J. Non-Cryst. Solids* **232–234** 300
[17] Hoppe U, Walter G, Barz A, Stachel D and Hannon A C 1998 *J. Phys.: Condens. Matter* **10** 261
[18] Suzuya K, Price D L, Loong C and Martin S 1998 *J. Non-Cryst Solids* **232–234** 650
[19] Grimmer A-R and Wolf G-U 1991 *Eur. J. Solid State Inorg. Chem.* **28** 221